Preferred citation: H.K. Corte and E.H. Lloyd. Fluid flow through paper and sheet structure. In **Consolidation of the Paper Web**, *Trans. of the IIIrd Fund. Res. Symp. Cambridge, 1965*, (F. Bolam, ed.), pp 981–1009, FRC, Manchester, 2018. DOI: 10.15376/frc.1965.2.981.

FLUID FLOW THROUGH PAPER AND SHEET STRUCTURE

H. K. CORTE and E. H. LLOYD, Wiggins Teape Research and Development Ltd., Beaconsfield, Bucks.

Synopsis—A theory is presented to describe the relationship between the structure of a sheet of paper and the flow of fluids through it. Based on the multi-planar concept of paper, it defines a pore through the sheet in terms of structural and hydrodynamic variables. The effective pore size distribution thus depends on the type of flow, as well as on the structure of the sheet. It is in all cases approximately lognormal, with a standard deviation proportional to the mean.

The theory is applied to the problem of the maximum pore size and to laminar flow, for which the connection with the Kozeny-Carman equation is established.

The theory correctly predicts relationships between physical and structural variables and fibre/sheet properties. Numerical agreement with experiments is still limited by the lack of an appropriate definition of a layer in the multi-planar model.

Introduction

THE PHENOMENON of fluid flow through porous materials has for a long time received considerable scientific and technological attention. It has produced a very substantial body of literature as one can see from the bibliography of Scheidegger's book,[1] published in 1957, which lists some 1 100 publications. The literature on fluid flow through paper, not counting test methods, amounts to little more than two dozen articles, most of which have been published since 1950.

Among the few articles published before that date is the one by Lucas,[2] who found the law of the capillary rise of liquids in paper and the one by Skraup *et al.*,[3] who studied the capillary rise of acids in paper.

The first of these two investigations aimed at finding the physical law controlling the process under consideration. Physical mechanisms were also largely the subject of articles by Ruoff *et al.*[4] (diffusion analogy of solvent flow in paper), Coupe & Smith[5] (penetration of printing ink), Kuniak[6] (penetration of water into pulp sheets), Hsu[7] (penetration of varnish into paper), Han[8] (aerosol filtration), Geitel[9] (flow through fibre plugs) and Napier[10] (oil penetration into paper).

The second of the two early articles mentioned above considers the interaction between the penetrating fluid and the paper. Such interactions formed part of the subject in articles by Peek[11] (contact angle from capillary rise), Vollmer[12] and Schaschek[13] (permeation of water vapour through paper) and Polčin[14] (liquid penetration into pulp sheets).

The fluid flow through paper is controlled, apart from interaction and physical laws of transport, by the structure of the sheet. This aspect is considered in articles by Tollenaar,[15] White & Marceau,[16] Bliesner[17] and in other publications referred to later. The structural aspect of porosity phenomena in paper was also presented by Corte[18] at the Cambridge symposium in 1957 and by Brecht[19] and Corte & Kallmes[20] at the Oxford symposium in 1961.

This paper offers for discussion an attempt to extend the statistical geometry of multi-planar sheets to determine some of the structural and physical factors that control the fluid flow through such sheets. The statistical geometry of paper was outlined by Corte & Kallmes[21] at the last symposium. It was also shown[20] how the concept of geometrical probability can be used to interpret physical properties in structural terms. Paper was considered to consist of a number of layers (multi-planar or MP structure), each having the structure of a two-dimensional fibre network (2-D sheet). In this way, it was possible for the first time to predict the results of physical experiments in terms of fibre and sheet dimensions alone.

One of the examples chosen was the determination of the maximum pore size of a sample of paper. The maximum pore size was found to be, in the first approximation, a simple function of the length density of the fibres, the substance of the paper and the area of the sample. The agreement between theory and experiment was encouraging. Further encouragement was drawn from the findings by Raďvan and co-workers, presented at this symposium, that paper cannot only be considered to have a layered structure, but does in fact have such a structure. It seemed feasible, therefore, to apply probability theory more rigorously to multi-planar sheets in order to describe their porous structure in more detail. Since quantitative results were aimed at, it was necessary to form a concept of a pore (a path of a fluid particle through paper) that was mathematically tractable and at the same time represented a fair approximation to reality.

The reality is, of course, an intricate network of interconnected voids and spaces between fibres, which may even form a coherent phase to which the concept of a pore in the normal sense of the word would be fundamentally alien. For a quantitative description of fluid flow through paper, however, the definition of a model is unavoidable. Well-known models are Kozeny's model and its variations, the 'drag theory' model and others. In order to define the model used in this article, paper is considered neither as an assemblage of fibres in a matrix of air (drag theory) nor as a two-phase system with the solid and gas phases penetrating each other (Kozeny's model), but as a multi-planar network of a known number of discrete fibres of known shapes separated by spaces that form the paths for the flow of fluid particles. In this way, the porous structure of paper, hence the fluid flow through it can be expressed in terms of fibre and sheet dimensions.

A particular application of the theory that we have in mind is to extract from the evaluation of experiments involving fluid flow more information than hitherto seemed possible about the structure of consolidated fibre networks, their degree and uniformity of compaction, two-sidedness, etc. Although the theory is still incomplete at the time of writing, it outlines in its present form the basis for such an approach.

Model and definition of a pore

THE MODEL considered here is best visualised in the form of a schematic cross-section through a multi-planar sheet (Fig. 1): The black areas are cross-sections of fibres, the white areas are cross-sections of spaces between them. The size of the latter in relation to that of the fibres is exaggerated.

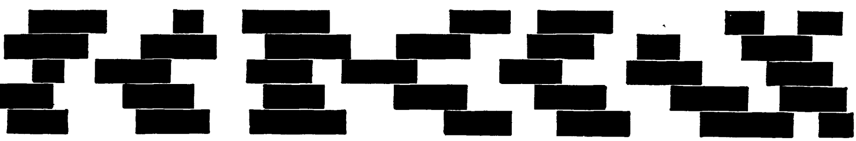

Fig. 1—Model of a multi-planar sheet

The sheet consists of m layers. Only vertical flow is considered and there is no horizontal flow between fibres in adjacent layers. The number of paths through the sheet n is equal to the number of pores (polygons) in one layer—that is, branching or splitting of paths is compensated by the blocking of others. A fluid leaves the sheet through as many openings on one side as it enters it on the other side.*

A *pore* is a path through the sheet consisting of a series of m openings of equal length. Its resistance to fluid flow is the sum of the resistances of the m openings. The openings are polygons whose sides are the free fibre lengths[21]

* Deviations from these definitions will be discussed in a later article: they cause the final expressions to be modified by terms of successive approximation, but do not affect the main argument

in one layer. The size of a polygon is defined by the radius r of a circle of equal area (see below). If the rate of fluid flow through an opening is proportional to the power k of its radius, its resistance to flow is proportional to r^{-k}. The resistance to flow of a series of m openings is proportional to $\sum_1^m r_i^{-k}$. The effective radius of a pore ρ is therefore defined as—

$$\rho_{m,k} = \left(\frac{m}{\sum_1^m r_i^{-k}}\right)^{1/k} \quad . \quad . \quad . \quad . \quad (1)$$

where r has the distribution of polygon radii in one layer.

The pore radius is thus defined by three parameters—

1. The mean free fibre length in one layer, which controls the polygon radius distribution. The mean free fibre length is in turn determined by the fibre dimensions and the statistical geometry of the layer as described [21]

2. The number of layers. This can be expressed by the substance of the sheet W and that of one layer G by $m = W/G$ . . . . (2)

3. The physical mechanism that controls the flow, expressed by the exponent k. For laminar, molecular, turbulent and capillary flow, we have $k=4$, 3, 2 and $\frac{1}{2}$, respectively.

The definition of the pore radius by equation (*1*) implies that the fluid flow through paper can be described by applying the appropriate transport equation to a system of n parallel cylindrical capillaries, n being the number of polygons in a layer of substance G. It is again determined by the fibre dimensions and the statistical geometry of the layer. Most of the remainder of this article is given to finding the distribution of the pore radius $\rho_{m,k}$.

Pore radius distribution

THE DISTRIBUTION of $\rho_{m,k}$ is found in two steps—

1. A rectangular grid model is introduced to approximate to the structure of a layer. The distribution of the polygon radius r for this model is derived. It is found to be approximately lognormal.

2. From this are successively derived the distributions of—

$$r^{-k}, \quad \left(\sum_1^m r_i^{-k}\right), \quad \left(\sum_1^m r_i^{-k}\right)^{1/k} \text{ and } \rho_{m,k}$$

As a result, the distribution of $\rho_{m,k}$ can be expressed in terms of m, k and the parameter of the basic grid.

Rectangular grid model

Whereas the distribution of the circumference of ν-sided polygons in a random network of lines is known to be χ^2 with $2(\nu-2)$ degrees of freedom,[22] the distribution of the polygon areas in such networks is unknown. It was shown in,[23] however, that the mean number of sides per polygon is 4. Furthermore, it is stated here without proof that the distribution of the polygon angle ϕ is $(1-\phi/\pi)\sin\phi$[24] and that the probability of a polygon being a triangle is $2-\pi^2/6 \approx 0.35$.[22] This means that 'roundish' polygons are much more frequent than oblong ones.

It was thought therefore that the polygon area distribution could be approximated by considering a rectangular grid of fibres that divides the plane into rectangular cells or pores. The sides of a typical pore represent free fibre lengths and have a negative exponential distribution with parameter $\gamma = 1/\bar{g}$, where $\bar{g}$ is the mean free fibre length of the layer. It should be noted that the distribution is independent of the fibre width as discussed previously.[23] Denoting by x and y the sides of a pore making a rightangle, we have therefore—

$$f(x) = \gamma\, \mathrm{e}^{-\gamma x} \quad \text{and} \quad f(y) = \gamma\, \mathrm{e}^{-\gamma y}; \quad x,y \geqslant 0$$

In order to find the distribution of the polygon area $a = xy$, we introduce—

$$\xi = \ln x; \quad g(\xi) = \gamma\, \mathrm{e}^{-\gamma x}\cdot \mathrm{e}^{\xi} = \gamma\, \mathrm{e}^{\xi}\cdot \mathrm{e}^{-\gamma \mathrm{e}^{\xi}}$$

Similarly— $\eta = \ln y; \quad g(\eta) = \gamma\, \mathrm{e}^{\eta}\cdot \mathrm{e}^{-\gamma \mathrm{e}^{\eta}} \quad -\infty < \xi,\eta < \infty$

Putting $\alpha = \xi + \eta$, we have—

$$h(\alpha) = \int_{-\infty}^{+\infty} g(\xi)g(\alpha-\xi)d\xi$$

$$= \gamma^2\, \mathrm{e}^{\alpha} \int_{-\infty}^{+\infty} \mathrm{e}^{-\gamma(\mathrm{e}^{\xi}+\mathrm{e}^{\alpha-\xi})}d\xi$$

or, with $\mathrm{e}^{\alpha} = a$ and $\phi(a) = \frac{1}{a}h(\alpha)$—

$$\phi(a) = \gamma^2 \int_{-\infty}^{+\infty} \mathrm{e}^{-\gamma(\mathrm{e}^{\xi}+a\mathrm{e}^{-\xi})}d\xi \qquad . \quad . \quad . \quad (3)$$

The integral in equation (*3*) was evaluated graphically and the distribution so obtained was compared with the results of a simulation on an IBM 1620 computer. We are very grateful to Dr O. Kallmes and Miss G. Bernier for providing data obtained from 584 random polygons. The mean free fibre

TABLE 1

Frequency	*Class (units)*				
	0–0.02	0.02–0.04	0.04–0.06	0.06–0.08	0.08 *and over*
Simulation	0.727	0.116	0.069	0.034	0.054
Equation (*3*)	0.668	0.152	0.072	0.038	0.070
Equation (*4*)	0.828	0.065	0.042	0.022	0.043

length in the experiment was $\bar{g}=0.159$ units. With this value, the results compare as shown in Table 1. The values in the last line of the table were calculated from an expression derived in a previous publication [equation (*26*)[23])], which can be written as follows—

$$\phi(a) = \frac{\gamma\sqrt{\pi}}{2}\cdot\frac{e^{-\gamma\sqrt{a\pi}}}{\sqrt{a}} \quad . \quad . \quad . \quad (4)$$

The grid model appears to be the better approximation. For this reason and another that will become apparent later, it was chosen for the calculation of the required polygon radius distribution.

The polygon radius (the radius of a circle of area equal to that of a rectangular polygon) is defined by—

$$r = \sqrt{xy/\pi} \quad . \quad . \quad . \quad . \quad (5)$$

We put $z=y$ and make the one-to-one transformation—

$$\left.\begin{array}{l} x = \pi r^2/z \\ \\ y = z \end{array}\right\}\begin{array}{ll} \dfrac{\partial x}{\partial r} = \dfrac{2\pi r}{z} & \dfrac{\partial x}{\partial z} = -\dfrac{\pi r^2}{z^2} \\ \\ \dfrac{\partial y}{\partial r} = 0 & \dfrac{\partial y}{\partial z} = 1 \end{array}$$

Since x and y are independent variables, the joint distribution $g(r,z)$ is then—

$$g(r,z) = f(x)\cdot f(y)\cdot\frac{\partial(x,y)}{\partial(r,z)}$$

The Jacobian has the value $2\pi r/z$, hence—

$$\begin{aligned} g(r,z) &= \gamma^2\, e^{-\gamma(x+y)}.\frac{2\pi r}{z} \\ &= \frac{2\pi r}{z}\gamma^2\, e^{-\gamma(r^2\pi/z+z)} \end{aligned}$$

Integration over z gives the distribution of the polygon radius as—

$$\begin{aligned} h(r) &= \int_0^\infty g(r,z)\, dz \\ &= 2\pi r\gamma^2 \int_0^\infty \frac{1}{z}\, e^{-\gamma(\pi r^2/z+z)}dz \\ &= 2\pi r\gamma^2 \int_0^\infty \frac{1}{z}\cdot e^{-\gamma\sqrt{\pi r^2}\,(\sqrt{\pi r^2}/z+z/\sqrt{\pi r^2})}\, dz \end{aligned}$$

We put $\qquad t = \dfrac{z}{\sqrt{\pi r^2}}$, that is, $t^{-1}\,dt = z^{-1}\,dz$

Therefore, $\qquad h(r) = 2\pi r\gamma^2 \displaystyle\int_0^\infty t^{-1}\, e^{-\lambda\sqrt{\pi r^2}(t+t^{-1})}\, dt$

Now, the modified Bessel function of the second kind (also known as the modified Hankel function) of degree ν is defined by—

$$K_\nu(\alpha y) = \tfrac{1}{2}\alpha^\nu \int_0^\infty e^{-\frac{1}{2}y(t+t^{-1})} t^{-1}\, dt$$

With $\nu=0$, $\alpha=1$, we have—

$$K_0(y) = \tfrac{1}{2}\int_0^\infty t^{-1}\, e^{-\frac{1}{2}y(t+t^{-1})}\, dt$$

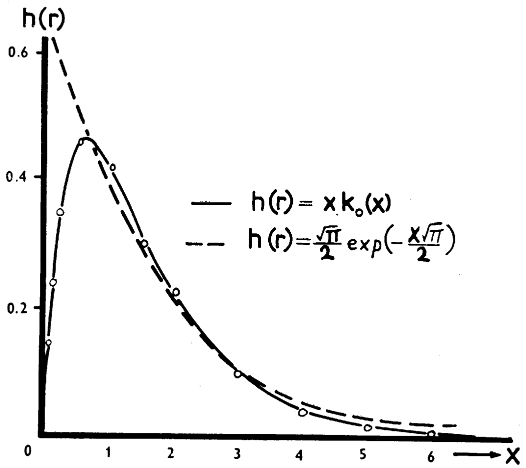

Fig. 2—Polygon radius distributions—see text, equations (*6*) and (*7*)

and with $\tfrac{1}{2}y=\gamma\sqrt{\pi r^2}$, it follows that—

$$2K_0(2\sqrt{\pi r^2}) = \int_0^\infty t^{-1}\, e^{-\gamma\sqrt{\pi r^2}(t+t^{-1})}\, dt = \frac{h(r)}{2\pi\gamma^2 r}$$

Finally, then $\qquad h(r) = 4\pi r\gamma^2 K_0(2r\gamma\sqrt{\pi})$

or $\qquad h(r) = bxK_0(x)$

with $\qquad b = 2\gamma\sqrt{\pi}$ and $x = br$ $\qquad$ . . . . (*6*)

The function $K_0(x)$ is tabulated.[25] Fig. 2 shows the distribution $h(r)$ for $b=1$ (that is, the unit on the abscissa is $2\sqrt{\pi/\bar{g}}$).

If equation (*4*) is transformed to $r=\sqrt{a/\pi}$, the resulting distribution is—

$$h(r) = \pi\gamma\, e^{-\pi\gamma r} \qquad . \quad . \quad . \quad . \quad (7)$$

This is the broken curve in Fig. 2. It is negative exponential with a maximum at zero radius, whereas the distribution (*6*) has a maximum defined by the equation—

$$\frac{dh\,(r)}{dr} = b\left[K_0(x)+x\frac{dK_0(x)}{dx}\right]\cdot\frac{dx}{dr} = b^2\left[K_0(x)-xK_1(x)\right] = 0$$

which is satisfied by $x=0.6$ (see Fig. 2).

It was found experimentally that pore radius distributions of paper, whatever the method of determination, have a maximum at a value of $r>0$. This is the first reason that the grid model is considered to be the better approximation. Another reason, closely related to the former and of some mathematical convenience is that the distribution derived from the grid model can be approximated reasonably well over a wide range by a lognormal distribution. This is shown in Fig. 3, where the cumulative of equation (*6*) is plotted on a logarithmic scale against x. The cumulative distribution is obtained from—

$$H(r) = \int_0^{br} xK_0(x)\,dx = \Big[-xK_1(x)\Big]_0^{br} = 1-brK_1(br)$$

The points lie almost on a straight line. This means that in this range $\ln r$ has a normal distribution with mean μ and standard deviation σ. The values of μ and σ are found from the mean and standard deviation of r, using the well-known relationships—

$$\left.\begin{aligned} E(r) &= e^{\mu+\frac{1}{2}\sigma^2} \\ \mathrm{Var}\,(r) &= E^2(r)\,(e^{\sigma^2}-1) \end{aligned}\right\} \quad . \quad . \quad . \quad (8)$$

According to the grid model, equation (*5*), we have—

$$E(r) = \frac{1}{\sqrt{\pi}}\cdot E(\sqrt{x})\cdot E(\sqrt{y}) = \frac{1}{\sqrt{\pi}}[E(\sqrt{x})]^2$$

Since
$$E(\sqrt{x}) = \gamma\int_0^\infty x^{\frac{1}{2}}e^{-\gamma x}\,dx = \gamma^{-\frac{1}{2}}\int_0^\infty u^{\frac{1}{2}}e^{-u}\,du$$

$$= \gamma^{-\frac{1}{2}}\Gamma(\tfrac{3}{2}) = \tfrac{1}{2}\sqrt{\pi/\gamma}$$

we have
$$E(r) = \sqrt{\pi}/4\gamma$$

Moreover,
$$E(r^2) = \frac{1}{\pi}E(xy) = \frac{1}{\pi}[E(x)]^2 = \frac{1}{\gamma^2\pi}$$

Hence,
$$\mathrm{Var}\,(r) = \frac{1}{\gamma^2}\left(\frac{1}{\pi}-\frac{\pi}{16}\right)$$

Inserting these values into equation (*8*), we obtain—

$$\left.\begin{aligned} e^{\sigma^2} &= 1 + \frac{\mathrm{Var}\,(r)}{E^2(r)} = \frac{16}{\pi^2} \\ e^{\mu} &= E(r)\,e^{-\frac{1}{2}\sigma^2} = \frac{\pi^{3/2}}{16\gamma} \end{aligned}\right\} \quad . \quad . \quad . \quad (8a)$$

Numerically, $\mu = -1.055 \ln \gamma; \quad \sigma^2 = 0.485 \quad . \quad . \quad . \quad (9)$

The result of the first step is that, in one layer, the logarithm of the polygon radius has approximately a normal distribution with mean and variance given by equation (*9*).

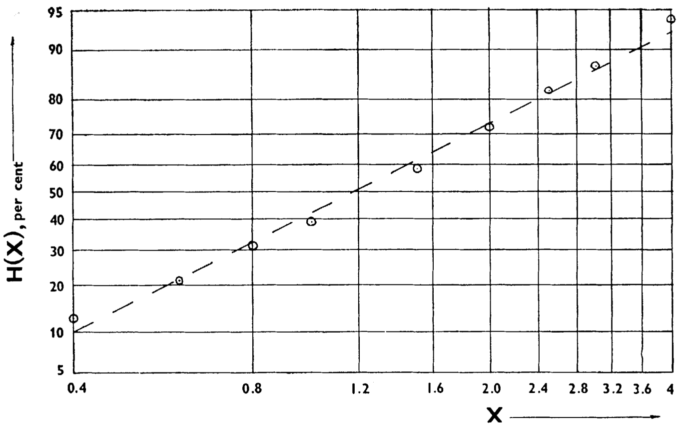

Fig. 3—Cumulative polygon radius distribution (grid model)

Multi-planar sheet

The convenient property of lognormal distributions is that powers of the variable are also lognormally distributed. In particular, if the distribution of $\ln r$ is normal (μ,σ), the distribution of $-k \ln r$ is normal with—

$$\mu_1 = -k\mu; \quad \sigma_1 = k\sigma \quad . \quad . \quad . \quad (10)$$

Thus, r^{-k} has a lognormal distribution.

The next distribution needed is that of $\sum_{i=1}^{m} r_i^{-k}$. Use is made here of another convenient property of lognormal distributions—the fact that they have the form of gamma distributions. One can easily show that the familiar χ^2 distribution (which is a rescaled gamma distribution) is very well represented by a lognormal distribution. This means that the addition law of gamma distributions can be applied to the distribution of r^{-k}.

The distribution of a variable u of type $\Gamma(c,n)$ is defined by—

$$f(u) = \frac{u^{n-1}\,\mathrm{e}^{-u/c}}{c^n\Gamma(n)}$$

Mean and variance are readily found to be—

$$E(u) = cn; \quad \mathrm{Var}\,(u) = c^2n$$

The addition law states that, if the variable u_1 is of type $\Gamma(c, n_1)$ and the variable u_2 of type $\Gamma(c,n_2)$, then the variable (u_1+u_2) is of type $\Gamma(c, n_1+n_2)$. Applying this to r^{-k}, we have the result that $\sum_{i=1}^{m} r_i^{-k}$ is of gamma type $\Gamma(c, mn)$, hence it has a lognormal distribution with—

$$E\left(\sum_{i=1}^{m} r_i^{-k}\right) = mE(r^{-k}) \quad \text{and} \quad \mathrm{Var}\left(\sum_{i=1}^{m} r_i^{-k}\right) = m\,\mathrm{Var}\,(r^{-k})$$

Mean and variance of the distribution of $\ln(\sum_{i=1}^{m} r_i^{-k})$, denoted by μ_2 and σ_2^2 are found as before, using the appropriate form of equations (*8*) and (*8a*). Instead of equations (*8*), we have—

$$\left.\begin{aligned} mE(r^{-k}) &= m\,\mathrm{e}^{\mu_1+\frac{1}{2}\sigma_1^2} = \mathrm{e}^{\mu_2+\frac{1}{2}\sigma_2^2} \\ m\,\mathrm{Var}\,(r^{-k}) &= m\,\mathrm{e}^{2\mu_1+\sigma_1^2}(\mathrm{e}^{\sigma_1^2}-1) = \mathrm{e}^{2\mu_2+\sigma_2^2}(\mathrm{e}^{\sigma_2^2}-1) \end{aligned}\right\} \quad (11)$$

Whence, in analogy to equation (*8a*)—

$$\left.\begin{aligned} \mathrm{e}^{\sigma_2^2} &= 1+\frac{\mathrm{Var}\,(r^{-k})}{mE^2(r^{-k})} = 1+\frac{1}{m}(\mathrm{e}^{\sigma_1^2}-1) = \frac{1}{m}\,\mathrm{e}^{\sigma_1^2}+\left(1-\frac{1}{m}\right) \\ \mathrm{e}^{\mu^2} &= mE(r^{-k})\,\mathrm{e}^{-\frac{1}{2}\sigma_2^2} = m\,\mathrm{e}^{\mu_1+\frac{1}{2}\sigma_1^2}\left[\frac{1}{m}\,\mathrm{e}^{\sigma_1^2}+\left(1-\frac{1}{m}\right)\right]^{-\frac{1}{2}}_{\mu_2} \end{aligned}\right\} \quad (11a)$$

Finally, the distribution of $\rho_{m,k}$ is found from that of $(\sum_{i=1}^{m} r_i^{-k})$ by using again the power law of lognormal distributions. Writing the defining equation (*1*) in the form—

$$\rho_{m,k} = \left(\frac{1}{m}\sum_{i=1}^{m} r_i^{-k}\right)^{-1/k} \quad . \quad . \quad . \quad (1a)$$

or

$$\ln \rho_{m,k} = -\frac{1}{k}\left(\ln \sum_{i=1}^{m} r_i^{-k} - \ln m\right) \quad . \quad . \quad . \quad (1b)$$

we see, that $\ln \rho_{m,k}$ is normally distributed with parameters (μ_3, σ_3), where—

$$\left.\begin{aligned} \mu_3 &= -\frac{1}{k}(\mu_2 - \ln m) \\ \text{and} \qquad \sigma_3 &= \frac{1}{k}\sigma_2 \end{aligned}\right\} \quad . \quad . \quad . \quad (12)$$

In analogy to equations (*8*), the mean and standard deviation are found to be—

$$\left.\begin{aligned} E(\rho_{m,k}) &= e^{\mu_3 + \frac{1}{2}\sigma_3^2} \\ \text{Standard deviation } (\rho_{m,k}) &= E(\rho_{m,k})\sqrt{e^{\sigma_3^2} - 1} \end{aligned}\right\} \quad . \quad (13)$$

If μ_3 and σ_3 are successively expressed by μ_2 and σ_2 from equations (*12*), μ_1 and σ_1 from equations (*11a*), μ and σ from equations (*10*) and the latter eliminated by equations (*8a*), equation (*13*) becomes—

$$\left.\begin{aligned} E(\rho_{m,k}) &= \frac{\pi^{3/2}}{16\gamma}\cdot\left(\frac{\pi}{4}\right)^k \left[\frac{\left(\frac{16}{\pi^2}\right)^{k^2} + m - 1}{m}\right]^{(k+1)/2k^2} \\ \text{Standard deviation } (\rho_{m,k}) &= E(\rho_{m,k})\cdot\left[\left(\frac{16}{\pi^2}\right)^{1/m}\cdot e^{(m-1)/mk^2} - 1\right]^{1/2} \end{aligned}\right\} \quad (14)$$

To the degree of approximation accepted in this discussion, the following more convenient expressions are sufficiently accurate—

$$\left.\begin{aligned} E(\rho_{m,k}) &= \frac{1}{3\gamma}\, e^{-\frac{1}{4}k}\left[\frac{e^{\frac{1}{2}k^2} + m - 1}{m}\right]^{(k+1)/2k^2} \\ \text{Standard deviation } (\rho_{m,k}) &= E(\rho_{m,k})\sqrt{e^{\sigma_2^2/k^2} - 1} \\ \text{where } e^{\sigma_2^2} &= \frac{1}{m}(e^{\frac{1}{2}k^2} - 1) + 1 \end{aligned}\right\} \quad (15)$$

The final result is that the pore radii in multi-planar sheets are approximately lognormally distributed with mean and standard deviation given by equations (*14*) or (*15*). The distribution has the following form—

$$f(\rho) = \frac{1}{\sigma_3\sqrt{2\pi}}\cdot\frac{1}{\rho}\cdot e^{-(1/2\sigma_3^2)(\ln \rho - \mu_3)^2} \quad . \quad . \quad (16)$$

where μ_3 and σ_3 (the parameters of the normal distribution of $\ln \rho$) are given by—

$$\left.\begin{aligned} \mu_3 &= -\frac{1}{k}\left\{-k\ln\frac{\pi^{3/2}}{16\gamma} + \frac{1}{2}k^2\ln\frac{16}{\pi^2} - \frac{1}{2}\ln\left[\frac{1}{m}\cdot\left(\frac{16}{\pi^2}\right)^{k^2} + \frac{m-1}{m}\right]\right\} \\ \sigma_3 &= \frac{1}{2k}\ln\left[\frac{1}{m}\left(\frac{16}{\pi^2}\right)^{k^2} + \frac{m-1}{m}\right] \end{aligned}\right\} \quad . \quad (17)$$

These equations state the relationship between the pore radius distribution on the one hand and the parameters γ, m and k on the other as discussed in connection with the definition of a pore, equation (*1*).

It was first noticed experimentally[18] that pore radius distributions of paper are lognormal with a maximum frequency at $\rho > 0$ and not at $\rho = 0$. This has since been widely confirmed, recently by Bliesner.[17] Corte[18] also found that, comparing a variety of paper grades over a wide range of porosities, the standard deviation of the distribution is proportional to the mean. This also was confirmed by Bliesner.[17]

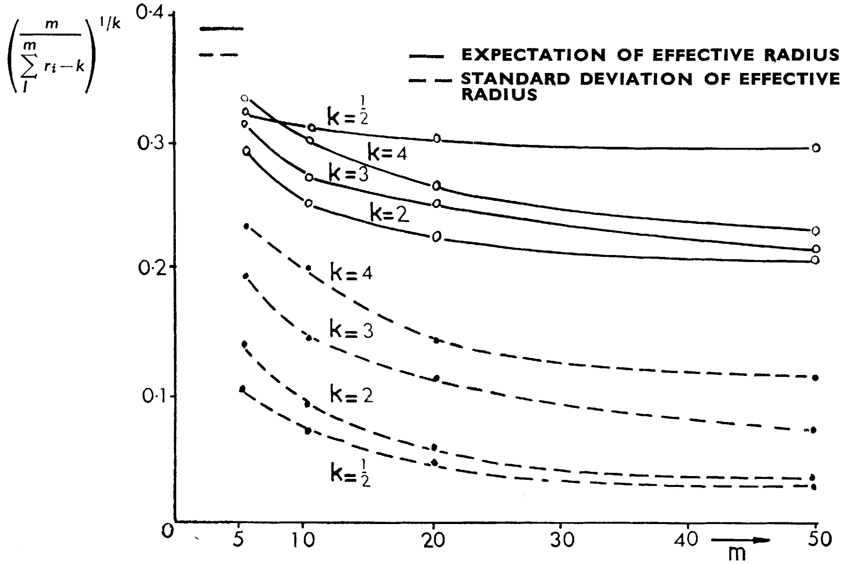

Fig. 4—Mean and standard deviation of pore radius distributions (unit = mean free fibre length)

Both results are given by the theory. The proportionality between standard deviation and mean follows from equation (*15*). The coefficient of variation is seen to be $\sqrt{e^{\sigma_3^2} - 1}$. From equation (*17*), it follows for laminar flow ($k = 4$) that the value is $(1.622m^{-1/16} - 1)^{1/2}$. The coefficient of variation is thus independent of γ and depends only little on m—that is, it is almost unaffected by fibre and sheet properties (for $m = 1$, 10, 25, 100, the values are 0.79, 0.63, 0.57, 0.47, respectively). The importance of this result is that more porous papers have not only larger, but also less uniform pores than denser papers. This fact, confirmed by general experience, is now recognised as a consequence of the basically random structure of the paper web as it is deposited on the machine wire and consolidated in the press and drying sections. Paper with large and uniform pores (as required for certain types of filter paper) cannot be made without interfering with the random structure. This property is readily achieved in the manufacture of a woven textile fabric or a metal wire mesh, which is the opposite of a random process.

A particular result of the theory is the effect of k, the type of fluid flow on the pore size distribution. Fig. 4 shows the mean and standard deviation as functions of m for four values of k, representing laminar, molecular, turbulent and capillary flow. Fig. 5 shows the resulting pore radius distributions for ($m=50$). In both graphs, the value $\gamma=1$ was used—that is, the unit of the ordinate of Fig. 4 and of the abscissa of Fig. 5 is the mean free fibre length of a layer.

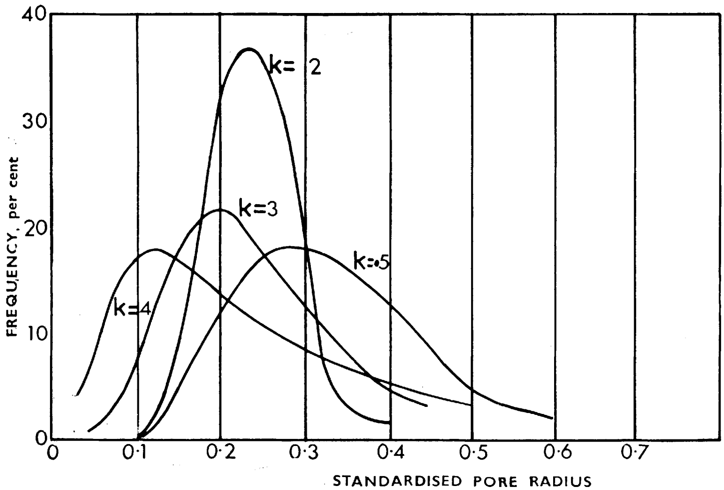

Fig. 5—Pore radius distributions (unit = free fibre length)

One notices that the same paper appears more open to capillary penetration of a liquid into it ($k=0.5$) than to laminar flow of the same liquid through it ($k=4$). Besides, it appears more uniform to turbulent flow ($k=2$) than to laminar flow. No experimental check of this behaviour was available at the time of writing.

Maximum pore size

WE DERIVE the expression for the radius of the largest pore, in order to compare it with the result presented in 1961.[20] The largest pore as determined by the 'first bubble' experiment was defined as follows. In each pore, consisting of m polygons in series, one of the polygons is the smallest (called bottleneck). There are n bottlenecks and the experiment gives the largest of them.

As stated earlier, the cumulative polygon radius distribution is—

$$H(r) = 1 - br \cdot K_1(br); \quad b = 2\gamma\sqrt{\pi} \qquad (18)$$

The probability that s is the smallest radius in a sample of m polygons is the probability that all m radii are larger than s—

$$P(S_m > s) = [1 - H(s)]^m$$

The cumulative distribution of bottleneck radii is therefore—

$$F(s_m) = 1 - [1 - H(s)]^m \qquad (19)$$

Of n bottleneck radii, the number of those larger than a given value r_0 is $n \times$ probability $(s_m > r_0)$ or $n[1 - F(r_0)]$. For a large value of n, a convenient definition of the 'expected largest' bottleneck, r_0 is given by making the last expression equal to unity. Thus, r_0 is defined by—

$$[1 - H(r_0)]^m = \frac{1}{n}$$

or, with equation (*18*), as—

$$2\gamma\sqrt{\pi} \cdot r_0 \cdot K_1(2\gamma\sqrt{\pi} \cdot r_0) = n^{-1/m} \qquad (20)$$

Fig. 6 shows r_0 in units of $\bar{g} = 1/\gamma$ as a function of m for four values of n. The curves are very nearly hyperbolic. Fig. 6 shows also that increases of n by factors of 10 add constant increments to r_0. This means that r_0 is proportional to $\log n$. Thus, the maximum pore radius is approximately inversely proportional to the number of layers (that is, the sheet substance for a given type of fibres) and directly proportional to the logarithm of n (that is, the sample area). The same result was found by Corte & Kallmes [equations (*8*) and (*11*)][20] using a negative exponential polygon radius distribution. It confirms the impression gained from Fig. 2 that the right tail of the polygon radius distribution is not far from negative exponential.

For a qualitative numerical estimation, we refer to an earlier publication,[21] equations (*5*)–(*7*), which, for the mean free fibre length, $\bar{g} = 1/\gamma$, give the expression—

$$\bar{g} = \frac{\lambda n_f}{2n_c} = \frac{2n_f \pi A}{2n_f^2 \lambda^2} = \frac{\pi A}{2n_f \lambda} = \frac{\pi w}{2G} \qquad (21)$$

Here, n_f and n_c are the numbers of fibres and fibre crossings in a layer of the sample, A its area and λ and w the mean length and length density of the fibres. The last member of equation (*21*) results from putting—

$$n_f \lambda w / A = G \quad . \quad . \quad . \quad . \quad (22)$$

which is the substance of the layer. Using equation (*2*), this becomes—

$$\bar{g} = \pi w m / 2W \quad . \quad . \quad . \quad . \quad (23)$$

If the relationship between $r_0/\bar{g}$ and m in Fig. 6 were hyperbolic of the type $r_0 m/\bar{g}$ = constant = C, we would have—

$$r_0 W = \pi/2 \times C \times w \quad . \quad . \quad . \quad . \quad (24)$$

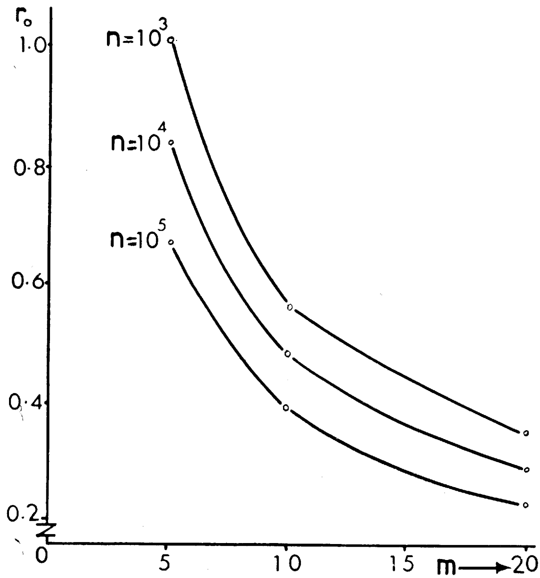

Fig. 6—Maximum effective radius as a function of thickness (m) for various sample sizes (n) (unit = mean free fibre length)

and the right side of this equation would correspond to the quantity K in the Corte & Kallmes equation (*12*).[20] In fact, C is not quite constant. For $10^3 < n < 10^4$, which is the range for samples of 10 cm² area, C varies between 4 and 6.5. Therefore, since w is of the order 2×10^{-6} g/cm, $r_0 W$ has values in the range 0.12–0.20, if the substance is given in g/m². The result agrees reasonably well with those reported in 1961.[20]

Laminar flow

ACCORDING to the model, the volume rate V of laminar fluid flow through a sheet is given by Poiseuille's equation for n pores of length l and radius distribution $f(\rho)$, equation (*16*)—

$$V = \frac{\pi p}{8\eta l}\cdot n\cdot E(\rho^4) \quad . \quad . \quad . \quad (25)$$

where ρ is the pressure and η the viscosity of the fluid. The fourth moment of the pore radius distribution $E(\rho^4)$ is given by—

$$E(\rho^4) = e^{4\mu_3 + 8\sigma_3^2}$$

By substituting successively equations (*12*), (*11a*), (*10*) and (*8a*), this becomes

$$E(\rho^4) = \left(\frac{\pi^{3/2}}{16\gamma}\right)^4\cdot\left(\frac{16}{\pi^2}\right)^{-8}\left[\frac{1}{m}\left(\frac{16}{\pi^2}\right)^{16} + \frac{m-1}{m}\right]$$

$$\approx \frac{0.7}{m}\bar{g}^4 \quad . \quad . \quad . \quad . \quad . \quad . \quad . \quad . \quad (26)$$

If in equation (*25*), the thickness of one layer (l) is replaced by L/m, where L = thickness of the sheet, equations (*25*) and (*26*) combine to give—

$$V = \frac{\pi p}{8\eta L}\cdot n\cdot 0.7\bar{g}^4 \quad . \quad . \quad . \quad (27)$$

Experimental checks were made by using air permeability data. The following units were used—V in cm^3/min, area = 10 cm^2, p = 100 mm water gauge, $\eta = 1.75\times10^{-4}$ poise. With these values, equation (*27*) reads—

$$V = 0.92\times10^9\times n/L\times\bar{g}^4 \quad . \quad . \quad . \quad (27a)$$

Both n and $\bar{g}$ depend numerically on the definition of a layer. The problem of a satisfactory definition of a layer has not yet been solved. Therefore, whereas trends of relationships between structure and flow are correctly predicted numerical agreement between theory and observation is at present only qualitative. This is particularly so in the case of equation (*27a*) because of the greatly magnified effect on the flow rate caused by even small variations of $\bar{g}$.

As an illustration we compare values for $\bar{g}$ calculated from equations (*21*) and (*27a*). From equation (*13*),[20] we quote the expression for n—

$$n = \frac{GA}{w}\left(\frac{G}{\pi w} - \frac{1}{\lambda}\right) e^{-G\omega/w} \quad . \quad . \quad . \quad (28)$$

where ω is the mean fibre width. A layer is here defined by its substance G, giving the same result for $\bar{g}$. A typical experimental result is the air permeability of 8.4×10^4 cm^3/min for a sheet made from unbeaten softwood sulphate pulp, of substance 30 g/m^2. The other data were $w = 1.8 \times 10^{-6}$ g/cm, $\omega = 3.9 \times 10^{-3}$ cm, $\lambda = 0.283$ cm, $L = 0.0075$ cm, $A = 10$ cm^2. Different values of G give the following values for $\bar{g}$, calculated from equations (*27a*) and (*21*)—

$G =$	1	6	10	15	25
Equation					
27a	$3.78 \cdot 10^{-3}$	$1.65 \cdot 10^{-3}$	$1.38 \cdot 10^{-3}$	$1.68 \cdot 10^{-3}$	$2.23 \cdot 10^{-3}$
21	$2.82 \cdot 10^{-2}$	$4.71 \cdot 10^{-3}$	$2.83 \cdot 10^{-3}$	$1.88 \cdot 10^{-3}$	$1.13 \cdot 10^{-3}$

According to the table, a layer would have a substance of about 15 g/m^2. Similar values were found for sheets made from different unbeaten or slightly beaten softwood or hardwood pulps. In the case of moderately or highly beaten pulps the G values were even higher.

Such high values for the substance of a layer can be interpreted as indicating only that the structure of a layer is denser and the mean free fibre length smaller than given by equation (*21*). This is probably due to the preferential penetration of fibres from adjacent layers into the wider openings of a given layer ('splitting') and the 'blocking' of preferentially smaller openings as mentioned earlier in connection with Fig. 1.

For the present discussion of general relationships between structural and physical variables, it is sufficient to define a layer as a slice of the sheet having a fractional open area $p(o)$ of the same value as the fractional void volume ϵ of the sheet. This makes a comparison with the Kozeny-Carman equation possible. The void volume is given[21] by—

$$\epsilon \equiv p(o) = e^{-G\omega/w}$$

whence

$$G = \frac{w}{\omega} \ln\left(\frac{1}{\epsilon}\right) \quad . \quad . \quad . \quad (29)$$

If we simplify equation (*28*) by considering fibres long enough to make $\frac{1}{\lambda} \ll \frac{G}{\pi w}$, we obtain—

$$n = \frac{G^2 A}{\pi w^2} \cdot \epsilon \quad . \quad . \quad . \quad . \quad . \quad (29a)$$

Thus, equation (*27*) becomes—

$$V = \frac{0.7}{128} \cdot \frac{\pi^4 p A}{\eta L} \cdot \frac{B^4 \epsilon \omega^2}{G^2}$$

or, with equation (*29*), it is—

$$V = \frac{0.7\pi^4}{128} \times \frac{pA}{\eta L} \times B^4 \frac{\epsilon}{\ln^2 (1/\epsilon)} \times \omega^2 \quad . \quad . \quad . \quad (30)$$

Here, an empirical factor $B<1$ is introduced on the right side of equation (*21*).

Kozeny-Carman's equation can be written as follows[25-27]—

$$V = \frac{pA}{L\eta} \times \frac{\epsilon^3}{5.55\, S^2(1-\epsilon)^2} \quad . \quad . \quad . \quad (31)$$

where S is the surface per unit volume of fibres. From a comparison of equations (*30*) and (*31*), it follows that—

$$\frac{\epsilon^2}{5.55(1-\epsilon)^2 S^2} = \frac{0.7\pi^4}{128}\omega^2 \frac{1}{\ln^2 (1/\epsilon)} \times B^4 \quad . \quad . \quad (32)$$

In our model, the specific surface S is given by—

$$S = \frac{\epsilon}{1-\epsilon} \times \frac{M}{\bar{g}} \quad . \quad . \quad . \quad . \quad (33)$$

where M is the mean numerical ratio of a polygon's circumference to its area in a layer. If $\bar{g}$ is again expressed by equations (*21*) and (*29*) and corrected by the factor B, one obtains—

$$S = \frac{\epsilon}{1-\epsilon} \times M \times \frac{2 \ln (1/\epsilon)}{B\pi\omega}$$

Introducing this in equation (*32*) gives—

$$M = 0.913/B^2 \quad . \quad . \quad . \quad . \quad (34)$$

The correct value of M for the grid model of a layer is given by—

$$M = 2E\left(\frac{x+y}{xy}\right) = 4E\left(\frac{1}{x}\right)$$

$$= 4\gamma \int_0^\infty \frac{1}{x} \mathrm{e}^{-\gamma x}\, dx = \infty$$

thus showing the limitations of this model at the boundaries. The value of M must, of course, remain finite, which means that the extremely small polygons for which M becomes large do not contribute to the flow. A more realistic value is the one of a square of side length $\bar{g}$ for which $M=4$. This would give $B \approx 0.48$. The correct derivation of B by an adequate definition of a layer is thus the problem that remains to be solved to complete the theory.

Conclusion

THE MULTI-PLANAR grid model leads to pore size distributions in accordance with general experience. The particular result that the effective pore size distribution depends on the mechanism of its determination is characteristic for the definition of a pore, which is partly structural, partly physical. Different types of fluid flow are described by using the appropriate moments of the pore radius distribution. Application of the theory to laminar flow gives formal agreement with the Kozeny-Carman equation.

The length density and/or width are the fibre properties of outstanding importance for fluid flow phenomena—a plausible result. Fibre length, on the other hand, is relatively unimportant so long as the fibres are not too short.

The concept of a layer, at present a somewhat arbitrary structural unit, has still to be defined more precisely in order to make numerical predictions from the theory possible.

ADDENDUM

Synopsis—Experimental results are presented to illustrate the effect of sheet density flocculation, fibre orientation and two-sidedness on the mean and standard deviation of the pore size distributions of handsheets made from different pulps. The effect of these variables, except fibre orientation, on the penetration of liquids was also investigated. The general agreement between the observed phenomena and the theoretical expectation lends further support to the validity of the chosen theoretical approach.

Introduction

AT the end of the introduction of our paper, it was pointed out that experiments involving fluid flow through paper should reveal structural features of the sheet that result from differing conditions of consolidation. Depending on these conditions, suspensions of the same kind of pulp fibres can be consolidated to give sheets of—

(*a*) Different densities (by applying different pressure).
(*b*) Different degrees of flocculation (by starting from suspensions with different concentrations).
(*c*) Different degrees of fibre orientation (by moving the wire at an angle to the direction of drainage).
(*d*) Different degrees of two-sidedness (by varying the suction and the conditions mentioned above).

The theory at present, based on the model illustrated in Fig. 1, refers to random, densely packed sheets. In order to interpret the results of fluid flow experiments in terms of the structural characteristics mentioned, it would need to be generalised. Before doing this, it is instructive to pose two questions—

1. Are the results of fluid flow experiments sensitive to differences in structure?

2. If so, will generalisations of the present theory, based on modified models, be likely to indicate the trends of these effects?

This addendum describes experiments designed to answer the two questions. The four structural effects mentioned above are discussed in turn.

1. *Effect of sheet density*

THE appropriate modification of the model (Fig. 1) to accommodate the effect of sheet density on fluid flow would be a separation of the layers in the vertical direction. Such a separation would clearly reduce the resistance to fluid flow and shift the distribution of the effective pore radius towards higher values. This is irrespective of the mathematical form in which this generalisation of the theory is expressed.

In order to investigate the effect of sheet density experimentally, two sets of handsheets were prepared: one set using a bleached softwood sulphate pulp and one set using a bleached hardwood sulphite pulp. Both pulps were slightly beaten. The fibre dimensions are listed in Table 2. The sulphate pulp fibres are coarser and tend to give bulkier and more porous sheets than do the hardwood sulphite fibres.

TABLE 2

Pulp	*Mean fibre length, cm*	*Mean fibre width, $cm \times 10^3$*	*Mean length density, $g/cm \times 10^6$*
Softwood sulphate	0.220	3.1	2.24
Hardwood sulphite	0.068	1.8	0.98

By applying different pressures and different pressing times on the British sheet-machine, sheets with different densities were made from both pulps. The basis weight was around 190 g/m^2. The pore size distributions were measured using the air permeation method described by Corte.[28] In this method, $k=4$ is used for evaluation. All of the distributions were approximately lognormal. Table 3 shows their means and standard deviations. The values are the averages of three determinations.

The results show a very pronounced reduction in pore size with increasing density, as one would expect. The logarithmic plot of the mean pore radius against the density (Fig. 7) can be approximated by straight lines, indicating a relationship of the form—

$$E(\rho_{m,4}) = d^{-\alpha} \qquad . \quad . \quad . \quad . \quad . \quad (35)$$

where d= density and $\alpha = 1.43$ for the softwood pulp and 1.38 for the hardwood pulp. This equation was used to eliminate the effect of density variations in experiments where the effects of other structural variables were studied. Since the

TABLE 3

Pulp	*Basis weight, g/m²*	*Density, g/cm³*	*Mean pore radius, cm × 10⁴*	*Standard deviation, cm × 10⁴*
Softwood sulphate	193	0.235	22.12	14.73
	195	0.422	10.45	6.40
	195	0.583	6.56	3.88
	192	0.690	4.72	2.64
Hardwood sulphite	190	0.294	8.48	4.48
	191	0.564	3.74	1.91
	190	0.636	2.77	1.55
	192	0.706	2.53	1.21

straight lines in Fig. 7 are nearly parallel, it follows that the ratio of the two mean pore radii at the same density is nearly constant. The average value in the density range 0.3—0.7 g/cm³ is 1.94. The ratio of the mean length densities of the fibres is 2.28 (Table 2). The difference, if real, means, according to equations (*15*) and (*21*), that one layer in the softwood sheets, whatever the definition, would have to be about 20 per cent heavier than in the hardwood sheets to be in formal agreement with the theory. Further experimental and theoretical work will be required to confirm such a result and to understand its meaning.

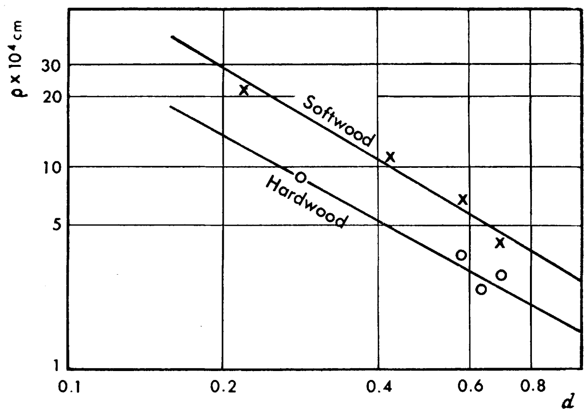

Fig. 7—Effect of density on mean pore size

The penetration of oil into sheets of two different densities 0.526 and 0.644 g/cm³ made from the softwood pulp was measured using a technique similar to the one described by Napier.[10] The difference here was that a limited amount of oil was applied. This penetrated the sheets only to 80—90 per cent of their complete saturation.

In Fig. 8, the depth of penetration (percentage of the sheet basis weight) is plotted against the square root of the time. According to Lucas,[2] a straight line should result for unrestricted penetration. The slopes decrease at higher degrees of penetration. This is due to a restriction to the flow, a result of the exhaustion of the oil supply. In spite of this effect, an increase in density reduces the rate of penetration, as one would expect.

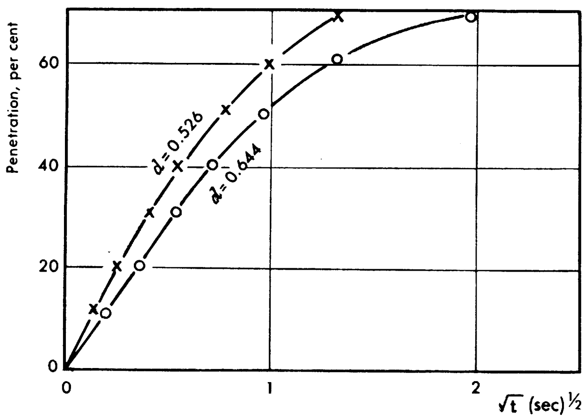

Fig. 8—Effect of density on oil penetration

For unrestricted capillary flow, $k = \frac{1}{2}$. Therefore, the ratio of the initial slopes should equal the square root of the ratio of the mean pore radii. From equation (*35*), this latter value for the densities 0.526 and 0.644 is 1.16. The ratio of the initial slopes is 1.27.

The result of this section is that an increase in sheet density retards both types of fluid flow ($k = 4$ and $k = \frac{1}{2}$).

2. *Effect of flocculation*

IN ORDER to accommodate the effect of flocculation, the model (Fig. 1) would have to be modified in that within each layer the fibre centres have a non-random distribution. By this, we mean that a layer is composed of regions having a grid spacing well above and others well below the average. Moreover, to ensure general flocculation, the pattern of flocculation in any one layer is repeated (or nearly so) through the thickness of the sheet.

In a gross simplification, such a sheet could be thought to consist of two regions—one in which the mean effective pore radius is x and one in which it is y. Each region covers, say, one half of the total area. Such a sheet would in principle behave like a pair of capillaries differing only in radii. A flocculated sheet is then represented by $x \gg y$ and a random sheet by $x \approx y$ or, to simplify manipulation, $x = y$.

The average flow rate through one capillary of the first pair ($x \gg y$) is given by—

$$\text{const. } \tfrac{1}{2}(x^k + y^k) \qquad (36)$$

The flow rate through one of the capillaries of the second pair ($x = y$), with a cross-sectional area equal to one half of the total cross-sectional area of the first pair, is given by—

$$\text{const.}\left(\sqrt{\frac{x^2+y^2}{2}}\right)^k \qquad (37)$$

where the constants are identical for equal values of k. For capillary flow ($k = \frac{1}{2}$), the 'average flow rate' means the average depth of penetration at a given time. If we now divide both expressions by the constant, substitute $x^2 = a$, $y^2 = b$ and $k = 2u$, then multiply them by 2^u, the first equation becomes—

$$2^{u-1}(a^u + b^u) \qquad (38)$$

and the second equation becomes

$$(a+b)^u \qquad (39)$$

For $a = b$, the two expressions are equal, regardless of the value of u. For $u = 1$, the two expressions are equal, regardless of the values of a and b. For $a \neq b$ and $u \neq 1$, it can be shown analytically that the first expression is always greater than the second one for $u > 1$ and smaller than the second one for $u < 1$. This means that the flow through the first pair of capillaries is the same as through the second pair if $k = 2$, that it is faster than through the second pair if $k > 2$ and that it is slower if $k < 2$.

It is obvious without further elaboration that the same result will be obtained when a set of pores covering a wide range of sizes (representing a flocculated sheet) is compared with a set of pores covering a narrower range of sizes (representing a more uniform or random sheet), provided both sets have the same total cross-sectional area. One would therefore expect that flocculation accelerates laminar and molecular flows ($k = 4$ and 3), retards capillary penetration ($k = \frac{1}{2}$) and does not affect turbulent flow ($k = 2$).

Only laminar and capillary flows were investigated. Handsheets of 100 g/m^2 basis weight were made from the two pulps used for the experiments in the previous section. Decreasing degrees of flocculation were produced by decreasing the concentration of the pulp suspension over a range of 1—0.01 per cent. Almost random sheets were made by couching together five layers of 20 g/m^2, each of which was made from a suspension of 0.002 per cent concentration. The degree of flocculation was assessed visually. The means and standard deviations of the pore size distributions were determined as described previously. Since the average sheet densities varied slightly around 0.45 g/cm^3, the mean pore radii were interpolated to this density, using equation (*35*). The standard deviations were corrected in proportion: Table 4 shows the results. Since the evaluation of the pore size distribution is based on the assumption of laminar flow, the mean pore radius is a direct measure of the resistance of the sheet to laminar flow. This resistance decreases with increasing flocculation. The effect is not very clear for the short-fibred hardwood pulp sheets, but remarkably pronounced for the long-fibred softwood pulp sheets.

Fig. 9 shows the penetration of oil into two sheets of different degrees of flocculation made from the softwood pulp. The oil penetrates more rapidly into the sheet with light flocculation than into the heavily flocculated sheet, in spite of its higher density. The sheets were made from suspension of 0.01 per cent and 1 per cent concentration, respectively.

TABLE 4

Pulp	*Concentration of suspension, per cent*	*Basis weight, g/m^2*	*Degree of flocculation*	*Mean pore radius, $cm \times 10^4$*	*Standard deviation, $cm \times 10^4$*
Softwood sulphate	0.0020	98	Layered	9.3	7.8
	0.0125	105	Light	11.0	6.5
	0.2	105	Medium	14.2	12.5
	1	109	Heavy	17.3	18.0
Hardwood sulphite	0.0020	83	Layered	11.1	4.7
	0.0125	87	Light	9.1	5.1
	1	84	Heavy	13.3	10.3

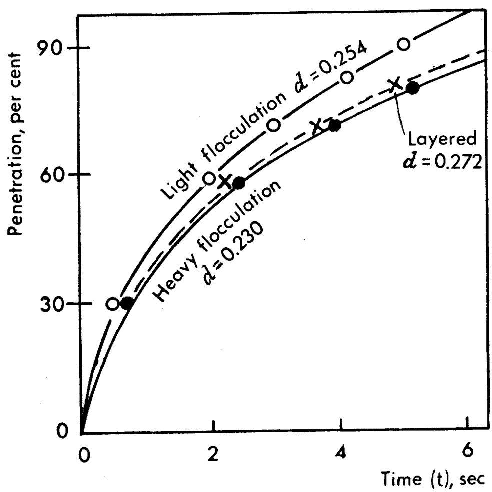

Fig. 9—Effect of flocculation

The result of this section is that, unlike the effect of density on the resistance to flow, that of flocculation depends on the type of flow: it accelerates laminar flow ($k = 4$), but retards capillary penetration ($k = \frac{1}{2}$).

3. *Effect of fibre orientation*

IN ORDER to accommodate the effect of fibre orientation, the model (Fig. 1) would have to be modified in that within each layer the fibre axes would have a preferred orientation. At the Oxford symposium, it was shown that the angular distribution of fibres can be described with sufficient accuracy by the first two terms of a Fourier series.(20) It was also shown that fibre orientation slightly increases the mean polygon area of a 2-D sheet. This is because the number of fibre crossings—hence, the number of polygons—is reduced by orientation. The effect was found to be small.

We had the good fortune that Mr G. Sauret from the Centre Technique de l'Industrie des Papiers, Cartons et Celluloses, Gières (France) very kindly supplied us with a number of sheets made on the centrifuge-type sheetmachine, developed to make anisotropic sheets and for which he published details.(29) We wish to express our sincere appreciation to Mr Sauret for his assistance.

TABLE 5

Degree of orientation	*Basis weight, g/m^2*	*Density, g/cm^3*	*Experimental*		*Corrected for density* 0.4	
			Mean pore size, $cm \times 10^4$	*Standard deviation, $cm \times 10^4$*	*Mean pore size, $cm \times 10^4$*	*Standard deviation, $cm \times 10^4$*
Zero	78	0.679	3.46	5.7	7.6	12.5
Low	71	0.368	10.90	8.4	9.5	7.3
Medium	83	0.375	9.10	6.7	8.4	6.2
High	73	0.389	5.20	4.1	5.0	3.9
Zero	122	0.403	2.41	1.6	2.4	1.6
Low	116	0.309	8.39	6.4	5.9	4.5
Medium	114	0.314	7.35	7.3	5.5	5.5
High	136	0.326	5.75	4.7	4.3	3.5

The sheets were made from slightly beaten bleached sulphite woodpulp. Two series were made—one of 80 g/m^2 and one of 120 g/m^2 nominal basis weight. Each series consisted of unoriented sheets and sheets with a low, medium and high degree of orientation. The sheets were extremely uniform in appearance and the different degrees of orientation were very apparent. The pore size distributions were determined as in the previous sections. Table 5 shows their means and standard deviations (averages of four determinations). The experimental mean pore radii show no discernible trend. In order to eliminate the effect of density variations, the values were corrected to a density of 0.4 g/cm^3, assuming that equation (*35*) applies to this pulp also. No improvement was achieved as the table shows. It is therefore concluded that the effect of fibre orientation on the pore size distribution is too small to be detectable by these fluid flow measurements. Oil penetration experiments were therefore not carried out.

4. Effect of two-sideness

IN ORDER to accomodate the effect of two-sidedness on fluid flow, the parameter γ in the rectangular grid model of one layer, characterising its mean spacing would vary with the depth of the layer. For example, γ could be higher in the central layers of the sheet than near the two surfaces—that is, the sheet could be denser in the centre than at the surfaces. If γ were the same at the surfaces, the sheet would then be symmetrical.

An unsymmetrical or two-sided sheet could be represented by a model similar to Fig. 1, in which the average grid spacing $1/\gamma$ increases from one side of the sheet to the other. If the relationship between depth and γ is, say, linear, such a sheet could, in a gross simplification, be thought to have conical pores. It would in principle behave like a truncated cone. If the radius of such a cone of length h_o varies from a value r_o at one end to $(r_o + ch)$ towards the other (c = a constant), its mean effective radius is given, according to equation (*1*), by—

$$\rho_{h_0,k} = \left[h_o \Big/ \int_0^{h_0} \frac{dh}{(r_o+ch)^k}\right]^{1/k} = \left[(k-1)ch_o \Big/ \left\{\frac{1}{r_o{}^{k-1}} - \frac{1}{(r_o+ch_o)^{k-1}}\right\}\right]^{1/k} \qquad (40)$$

This expression is independent of the direction of flow—that is, of the sign of c. It reduces $\rho_{h_0,k} = r_o$ for $c = 0$.

The rate of laminar flow through such a truncated cone is independent of its direction. (This is, strictly speaking, true only for incompressible fluids, but we assume it to be approximately true for gases also, if the pressure difference is kept small. The physical complications that arise when the fluid is compressible are not discussed here, because they do not affect the principal argument.) The rate of capillary penetration, however, depends obviously on the direction.

Consider a liquid of viscosity η and interface tension with the pore wall σ rising vertically into the conical pore defined above. The relationship between the height of capillary rise h and the time t is given by—

$$h^2(c^2h^2 + 4r_och + 6r_o{}^2) = \frac{3\sigma}{\eta} r_o{}^3 t \qquad (41)$$

This means, as one can easily verify, that the liquid penetrates faster into a converging capillary (c negative) than into a diverging one (c positive) of the same dimensions. For $c = 0$, equation (*41*) reduces to Lucas' familiar equation (*2*)—

$$h^2 = \frac{\sigma r}{2\eta} t \qquad (42)$$

Both equations are valid only for values of h well below the equilibrium height. For the penetration of liquids into paper, this condition is always fulfilled.

For easier comparison with experiments described later, let us also consider a laminated sheet consisting of a top half with large γ and a bottom half with small γ. Such a sheet would in principle behave like two capillaries in series. Consider such a set with radii r_1 and r_2, corresponding to those at the ends of the conical capillary. Let the lengths be equal and the total length be the same as the length of the conical capillary.

The mean effective radius in the case of laminar flow is, according to equation (*1*), given by—

$$\rho_{2,4} = r_1 r_2\left(\frac{2}{r_1^4 + r_2^4}\right)^{1/4} \qquad (43)$$

The flow rate is again independent of the direction.

Liquid penetration into the first capillary of radius r_1 is described by equation (*42*) with $r = r_1$ and into the second by—

$$\frac{h^2}{2} - h_1\left(1 - \frac{r_2^4}{r_1^4}\right)h = \frac{\sigma r_2}{4\eta}t \qquad (44)$$

where h_1 is the length of the first capillary. The rate of penetration dh/dt at this height changes discontinuously from $\frac{\sigma r_1}{4\eta h_1}$ at the end of the first capillary to $\frac{\sigma r_2}{4\eta h_1}\cdot\frac{r_1^4}{r_2^4}$ at the beginning of the second capillary. If $r_1 > r_2$ (convergent flow), the latter rate is higher than the former—that is, the liquid is accelerated when it reaches the second capillary. If $r_1 < r_2$ (divergent flow), the reverse is true and the liquid is additionally retarded.

TABLE 6

Composition of sheet and direction of flow	*Basis weight, g/m²*	*Mean pore radius, cm × 10⁴*	*Standard deviation, cm × 10⁴*
Softwood	98	10.22	9.3
Hardwood	96	6.05	6.1
Soft→Hard	202	6.11	4.6
Hard→Soft	206	6.32	4.2
Soft→Hard→Soft	297	6.97	5.0

In order to check these simplified considerations experimentally, laminated handsheets were made by couching together sheets of approximately 100 g/m² basis weight made from the pulps used for the other series of experiments. The pore size distributions, determined as in the previous experiments, had means and standard deviations as listed in Table 6. The figures are the averages of three determinations and corrected to a density of 0.45, using equation (*35*).

It will be noticed that the mean pore sizes of the composite sheets are largely determined by their denser layers as one would expect from equation (*43*). The direction of flow has no appreciable influence on the effective pore sizes.

In order to illustrate equations (*41*) and (*44*), theoretical penetration curves are plotted in Fig. 10*a*. The following numerical values were used—

Converging cone: $r_o = 10 \times 10^{-4}$ cm; $c = -2.5 \times 10^{-2}$
Converging step change: $r_1 = 10 \times 10^{-4}$ cm; $r_2 = 5 \times 10^{-4}$ cm
Diverging cone: $r_o = 5 \times 10^{-4}$ cm; $c = 2.5 \times 10^{-2}$
Diverging step change: $r_1 = 5 \times 10^{-4}$ cm; $r^2 = 10 \times 10^{-4}$ cm
Total: $h_1 = 0.01$ cm; $\eta = 1.3$ poise, $\sigma = 2.8$ dyn/cm.

One can see the different direction of the sudden change in flow rate when the liquid reaches the second capillary: acceleration if the flow is convergent (upper curve), retardation if it is divergent (lower curve). One can also see that these curves resemble closely those for the convergent and divergent cones.

A study was made of the penetration of oil into sheets similar to those of Table 6: Fig. 10*b* shows the results. The curves are averages of three measurements. The direction of flow affects the penetration in much the same way as the capillary model predicts, although the absolute penetration rates are much smaller than in the models.

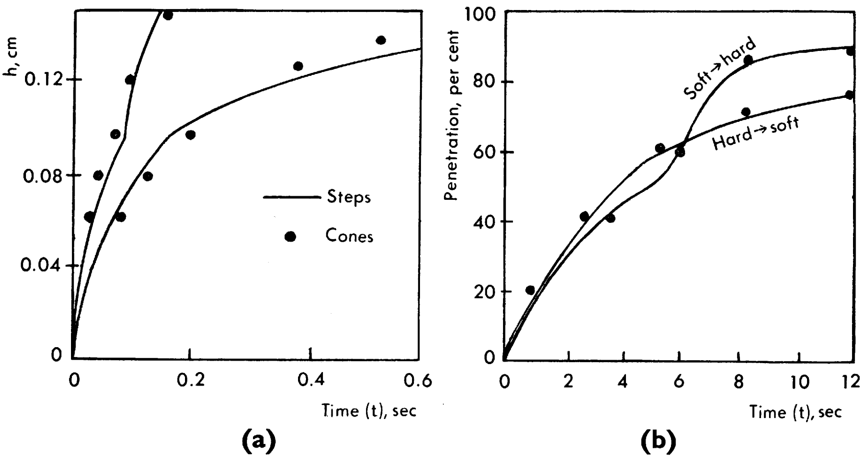

Fig. 10—Effect of two-sidedness on oil penetration

The result of this section is that, in two-sided sheets, laminar flow does not depend on the direction; the mean effective pore size is largely determined by the denser layers of the sheet; capillary penetration is faster when the liquid moves from the more open to the more closed side of the sheet than vice versa.

5. *Coefficients of variation*

THE coefficients of variation did not reveal anything unexpected. They are between 0.6 and 1, with higher values for flocculated sheets. They were remarkably constant in the experiments on the effect of density (section 1).

Conclusion

THE experimental results presented here must be considered as preliminary. More pulps will have to be tested under a wide range of conditions before quantitative conclusions can be drawn and fluid flow experiments be used to study sheet structure. The fact that a variety of predictions is confirmed by experiments, however, is encouraging enough to answer the two questions posed at the beginning as follows—

1. Fluid flow measurements are sensitive to differences in density, flocculation and two-sidedness, but not in fibre orientation.

2. The present theory seems capable of such generalisations as to include these structural characteristics, which in turn are largely determined by the conditions of the consolidation of the web.

References

1. Scheidegger, A. E., *The Physics of Flow through Porous Media* (University Press, Toronto, 1957)
2. Lucas, R., *Kolloid-Z.*, 1918, **35**, 15–22
3. Skraup, Zd. H., Krause, E. and Biehler, A. v., *Monatshefte f. Chemie*, 1910, **31**, 753–776
4. Ruoff, A. L., Prince, D. L., Giddings, J. C. and Stewart, G. H., *Kolloid-Z.*, 1959, **166** (2), 144–151
5. Coupe, R. R. and Smith, A. H., *J. Oil Col. Chem. Assoc.*, 1956, **39** (8), 579–608
6. Kuniak, L., *Svensk Papperstidn.*, 1962, **65** (19), 760–766
7. Hsu, B., *J. Coll. Sci.*, 1963, **18** (1), 41–51
8. Han, S. T., *Tappi*, 1964, **47** (12), 782–787
9. Geitel, K., *Faserforschung u. Textiltechnik*, 1964, **15** (1), 21–29
10. Napier, J. D., *Paper Tech.*, 1964, **5** (3), T99–T104
11. Peek, R. L. Jnr. and McLean, D. A., *Ind. Eng. Chem.* (*Anal. Ed.*), 1934, **6** (2), 85–90
12. Vollmer, W., *Chem. Ing. Techn.*, 1954, **26** (2), 90–94
13. Schaschek, H., *Chem. Ing. Techn.*, 1956, **28** (11), 698–702
14. Polčin, J., *Sbornik VUPC*, 1960, **5**, 185–209
15. Tollenaar, D., *Appl. Sci. Res.*, 1952, **A3**, 451–461
16. White, R. E. and Marceau, W. E., *Tappi*, 1962, **45** (4), 279–284
17. Bliesner, W. C., *Tappi*, 1964, **47** (7), 392–400
18. Corte, H., *Fundamentals of Papermaking Fibres*, Ed. F. Bolam (Technical Section, B.P. & B.M.A., Kenley, 1958), 301–331
19. Brecht, W., *Formation and Structure of Paper*, Ed. F. Bolam (Technical Section, B.P. & B.M.A., London, 1962), 427–460
20. Corte, H. and Kallmes, O., *Formation and Structure of Paper*, Ed. F. Bolam (Technical Section, B.P. & B.M.A., London, 1962), 351–368
21. Corte, H. and Kallmes, O., *Formation and Structure of Paper*, Ed. F. Bolam (Technical Section, B.P. & B.M.A., London, 1962), 13–46
22. Miles, R. E., *Proc. Nat. Acad. Sci.*, 1964, **52** (4), 901–907; (5), 1157–1160
23. Kallmes, O. and Corte, H., *Tappi*, 1960, **43** (9), 737–752
24. Stone, M., private communication
25. Carman, P. C., *Trans. Inst. Chem. Eng.* (*London*), 1937, **5**, 150–166
26. Fowler, J. L. and Hertel, K. L., *J. appl. Phys.*, 1940, **11** (7), 496–502
27. Sullivan, R. R., *J. appl. Phys.*, 1941, **12** (6), 503–508
28. Corte, H. K., *Das Papier*, 1965, **19** (7), 346–351
29. Sauret, G., *ATIP Bull.*, 1962, **16** (6), 446–452

Discussion

Mr P. E. Wrist—Your thesis is that the mean size of the pores varies with the uniformity of the sheet and therefore with the degree of flocculation. As the degree of flocculation worsened, you will find a larger average pore size. A corollary of this is that there must be fewer fibres per unit area at each level through the sheet, since the average pore size can increase only if there is a decrease in the total number of pores at each level. For a sheet of given substance, therefore, the non-uniform sheet must consist of more levels or layers than the uniform sheet. In other words, the non-uniform sheet will have the greater caliper. Is this deduction observed in practice?

Dr H. K. Corte—The caliper does not really matter in this connection. What I said was that the average size or the effects of increasing flocculation on the average pore size depend on the method by which you determine the pore size. It is found to be larger for flocculated sheets than for uniform sheets of the same density when the flow mechanism used to determine it is as in a laminar flow. It is smaller, however, when the flow is capillary. It is independent of the degree of flocculation when the flow is turbulent.

Dr C. K. Meadley—It seems to me that the only thing remaining to provide a final rigorous treatment is the non-arbitrary definition of a layer. Have you any further thoughts for future work to rationalise this concept?

Dr Corte—I mentioned at the beginning that the horizontal flow was neglected and its inclusion caused us some trouble and this is in fact connected with the definition of a layer. So far, we have not found a non-arbitrary definition and it seems to me that we will have to introduce some physical definition, just as we had to define the size of the pore physically, but this has not yet been achieved.